Int. J. Electrochem. Sci., 12 **(2017)** 9051 – 9060, doi: 10.20964/2017.10.62

International Journal of
ELECTROCHEMICAL
SCIENCE
www.electrochemsci.org

Effect of Aluminum Doping on the Stability of Lithium-Rich Layered Oxide $Li[Li_{0.23}Ni_{0.15}Mn_{0.52}Al_{0.10}]O_2$ as Cathode Material

Yun-Peng Zhang[1,3], *Er-Qian Liang*[1,3], *Jin-Xia Wang*[1,3], *Bao-Jun Yu*[2,3], *Cheng-Yang Wang*[2,3], *Ming-Wei Li*[1,3,*]

[1] Department of Chemistry, Tianjin University, Tianjin 300072, China
[2] Key Laboratory for Green Chemical Technology of Ministry of Education, School of Chemical Engineering and Technology, Tianjin University, Tianjin 300072, China
[3] Collaborative Innovation Center of Chemical Science and Engineering (Tianjin), Tianjin University, Tianjin 300072, China
[*]E-mail: mingweili@tju.edu.cn

Received: 5 June 2017 / *Accepted:* 9 August 2017 / *Published:* 12 September 2017

Lithium-rich layered oxide $Li[Li_{0.23}Ni_{0.15}Mn_{0.62}]O_2$ and its Al-doped product $Li[Li_{0.23}Ni_{0.15}Mn_{0.52}Al_{0.10}]O_2$ are synthesized via a sol−gel and calcining method, and are used as the cathode materials for lithium-ion batteries. Both samples show a layered α-$NaFeO_2$ structure with $R\bar{3}m$ symmetry. Compared with $Li[Li_{0.23}Ni_{0.15}Mn_{0.62}]O_2$, $Li[Li_{0.23}Ni_{0.15}Mn_{0.52}Al_{0.10}]O_2$ shows better crystallinity, and exhibits more stable capacities and better rate performance during cycling. It possesses a capacity of >180 mAh g^{-1} at the current density of 20 mA g^{-1}, and displays nice capacity retention after rapid charging/discharging. Although the doped aluminum in $Li[Li_{0.23}Ni_{0.15}Mn_{0.52}Al_{0.1}]O_2$ does not show obvious redox during cycling, it enhances the structural and electrochemical stability of the lithium-rich layered oxide.

Keywords: Cathode material; Lithium-rich layered oxide; Aluminum doping; Electrochemical performance

1. INTRODUCTION

Today, lithium-ion batteries are widely applied in portable electronic devices due to their high energy densities, low self-discharge, and tiny memory effect [1]. However, the first commercialized cathode material, $LiCoO_2$, is suffering high cost, toxicity, and safety problems. Besides the commercialized nickel-manganese-cobalt oxide, other similar layered structure materials, such as $LiNiO_2$, $LiMnO_2$, $LiMn_2O_4$, and so on, have been widely studied as the potential cathode materials [2−15]. But they have some flaws as being cathode materials. It was reported that $LiNiO_2$ is difficult to

be synthesized, and its capacity rapidly decays due to the formation of NiO_2 phase [2,3]. The exothermic decomposition of $LiNiO_2$ in charged state at a higher temperature raises safety concerns. $LiMnO_2$ is unstable as its layered structure transforms to a spinel structure during cycling [4,5]. $LiMn_2O_4$ also suffers severe capacity fade at high temperature, Jahn-Teller distortion of Mn^{3+}, manganese ions dissolution in electrolyte, formation of two cubic phases and development of microstrain [6,13]. $LiNi_{0.5}Mn_{0.5}O_2$ material has been extensively investigated since the first report in 1997 [2,9]. It has a highly reversible capacity, good cyclic performance, and excellent thermal stability. Compared with $LiNiO_2$ and $LiMnO_2$, $LiNi_{0.5}Mn_{0.5}O_2$ does not transform to a spinal structure during cycling and doesn't have sign of structure degradation due to multiphase reaction at high voltage [9,12,14]. Simultaneously, $LiNi_{0.5}Mn_{0.5}O_2$ also has high thermal stability and low toxicity. But $LiNi_{0.5}Mn_{0.5}O_2$ has inherent disadvantages such as unstable characteristic at a high voltage (> 4.3 V), structural impurities, and existing substantial Li/Ni cation mixing [15,16].

Various metals such as Co, Al, Mg, Fe, Zn, and Ti were doped in Li−Ni−Mn−O system, and effectively improve the electrochemical performance of cathode materials [11,13−19]. Specially, it was reported that Al-doped $LiNi_{0.475}Mn_{0.475}Al_{0.05}O_2$ reduces the cation mixing of $LiNi_{0.5}Mn_{0.5}O_2$, which may overcome the initial irreversibility and enhance the cycling performance of cathodes [7]. The Al-contained $LiNi_{0.475}Mn_{0.475}Al_{0.05}O_2$ shows improved discharge capacities from 120 to 142 mAh g^{-1} [8]. The Al-doped $LiNi_{0.8}Co_{0.2}O_2$ also possesses modified cycle lifetimes and thermal stability [9].

It was reported that the lithium-doped Li−Ni−Mn−O oxide called lithium-rich layered oxide, such as $Li[Li_{0.23}Ni_{0.15}Mn_{0.62}]O_2$, can deliver high capacities (>200 mAh g^{-1}) [20−27]. The lithium-rich oxide has a layered structure with an interlayer spacing of ~0.47 nm, which facilitates the transferring of lithium ions during charging/discharging. The layered structure is built by transition metal layers and lithium layers. The transition metal layer consists of MO_6 (M = Mn, Ni, Li) octahedra. Not only all manganese and nickel but also partial lithium (i.e., the "rich lithium") are located in the transition metal layers [25−27]. It is widely accepted that the lithium-rich layered oxide rearranges its structure during the initial charge at a high voltage (~4.6 V), and possess high capacities. We think that lithium-rich layered oxide is a potential cathode material in industry.

Various methods, including hydrothermal method, sol−gel method, spray-drying method, co-precipitation, and electrospinning method, have ever been applied to prepare the doped Li−Ni−Mn−O materials or their precursors. Among them, the sol−gel method is one simple route without multistep process, and does not suffer metal ions loss.

In this paper, we synthesized two lithium-rich layered oxides, $Li[Li_{0.23}Ni_{0.15}Mn_{0.62}]O_2$ and its Al-doped product $Li[Li_{0.23}Ni_{0.15}Mn_{0.52}Al_{0.10}]O_2$, via sol−gel method following by a calcining process. Their crystal structures and cathode performance are studied. The Al-doped lithium-rich layered oxide shows more stable capacities during cycling, and exhibits improved rate performance.

2. EXPERIMENTAL

The precursors of two lithium-rich layered oxides, $Li[Li_{0.23}Ni_{0.15}Mn_{0.62}]O_2$ and Al-doped $Li[Li_{0.23}Ni_{0.15}Mn_{0.52}Al_{0.10}]O_2$, were synthesized via a sol−gel method by using citric acid as the

chelating agent. The main raw materials include $LiNO_3$, $Ni(NO_3)_2 \cdot 6H_2O$, $Mn(NO_3)_2$, $Al(NO_3)_3 \cdot 9H_2O$, and $C_6H_8O_7 \cdot H_2O$. Stoichiometric raw materials were dissolved in distilled water. The molar ratio of citric acid to total metal ions was 1:1. The solution's pH value was adjusted in a range of 8.0–9.0 by ammonium hydroxide solution. After being continuously stirred at 80 °C for about 24 h, the mixed solution was evaporated at 80 °C until a dried gel forming. The gel was dried in a vacuum oven at 120 °C for 24 h. The precursor was heated at 1 °C min^{-1} to 800 °C and held at800 °C for 12 h before cooling.

The synthesized samples were analyzed by a powder X-ray diffractometer (Rigaku D/Max 2200 PC) using Cu Kα radiation (λ= 0.15418 nm). The samples' morphology and structure were recorded by a field emission scanning electron microscope (SEM, S4800, HITACHI) and a high-resolution transmission electron microscope (HRTEM, JEM-2100F, JEOL). Their electrochemical properties were measured using CR2430-type coin cells with metallic lithium served as anode electrodes. The cathode electrodes were prepared by coating slurry on aluminum current collector foil. The slurry consists of 80 wt% active material, 10 wt% Super P carbon black, and 10 wt% polyvinylidene fluoride using N-methyl-2-pyrrolidone as a solvent. The electrodes were dried at 120 °C under vacuum. $LiPF_6$ (1.0 M) in ethylene carbonate-dimethyl carbonate (1:1 in volume) and microporous polypropylene film (Cellgard 2400) were used as the electrolyte and separator, respectively. The galvanostatic discharge/charge tests were performed on a battery program control test system (LAND CT2001A, China) between 2.0 and 4.8 V at a current density 20 mA $h \cdot g^{-1}$. The rate capability was tested at a current density range from 20 to 600 mA$\cdot g^{-1}$. The cyclic voltammetry (CV) measurement was carried out by an electrochemical working station (CHI604E, CH Instruments, China) at a scanning rate of 0.1 mV$\cdot s^{-1}$ from 2.0 to 4.8 V.

3. RESULTS AND DISCUSSION

Fig. 1 presents the synthesized samples' XRD patterns. Either sample possesses a layered α-$NaFeO_2$ structure with a space group of $R\bar{3}m$ symmetry, in which the iron sites are occupied by Ni, Mn, Al and Li, and the sodium sites by Li [13]. The diffusion peaks between 20° and 25° indicate trace monoclinic Li_2MnO_3 with a space group of $C2/m$ existing in the samples. No other impurity-related peaks are observed. The samples are composed of a main trigonal system and a trace monoclinic system, which agrees with previous reports [25,26]. According to literature [8,20], Li_2MnO_3 originates from the random stacking of layers, and may enhances the material stability during cycling. Compared with the XRD pattern of $LiNiO_2$, whose close diffusion peak couples (006) and (012), and (108) and (110) almost overlap, the two double peak couples for either synthesized sample are splitting. It possibly results from the different ion sizes of Al^{3+} (0.535 Å) and Mn^{4+} (0.53 Å) than that of Ni^{6+} (0.69 Å). Generally, smaller foreign ion Al^{3+} can easily dope into the host crystals. The lattice parameters of samples are showed in Table 1. The intensity ratio of I_{003}/I_{104} for two samples are above 1.2, implying the undesirable cation mixing being suppressed [18]. Compared with $Li[Li_{0.23}Ni_{0.15}Mn_{0.62}]O_2$, the Al-doped sample shows less different lattice parameters, implying a successful doping. The results prove that Al easily dopes the lithium-rich layers oxide via a simple sol−gel and calcining method. The

bonding energy of Al−O bonds (512 kJ mol^{-1}) is higher than that of Ni−O bonds (392 kJ mol^{-1}) and Mn−O bonds (402 kJ mol^{-1}) [28]. So the synthesized $Li[Li_{0.23}Ni_{0.15}Mn_{0.52}Al_{0.10}]O_2$ may possess a more stable crystal structure.

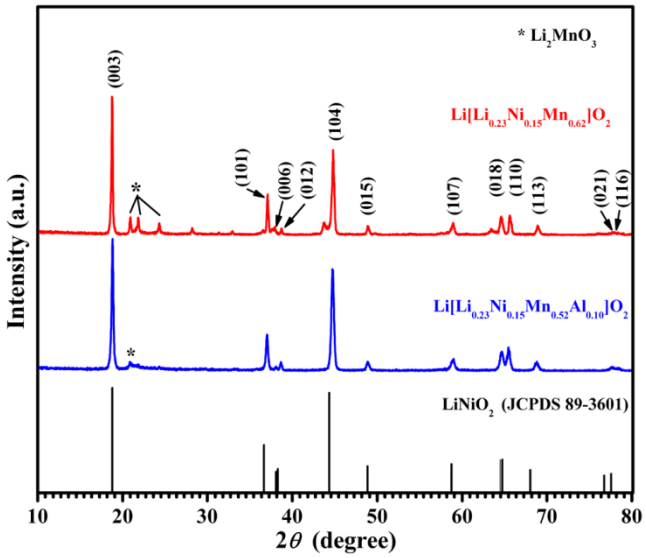

Figure 1. XRD patterns for the synthesized $Li[Li_{0.23}Ni_{0.15}Mn_{0.62}]O_2$ and $Li[Li_{0.23}Ni_{0.15}Mn_{0.52}Al_{0.10}]O_2$ samples.

Table 1 Lattice parameters of the synthesized samples

	$Li[Li_{0.23}Ni_{0.15}Mn_{0.62}]O_2$	$Li[Li_{0.23}Ni_{0.15}Mn_{0.52}Al_{0.10}]O_2$
a (Å)	2.8472	2.8537
c (Å)	14.2453	14.2336
I_{003}/I_{104}	1.6329	1.2873
c/*a*	5.0033	4.9878
Unit volume ($Å^3$)	100.01	100.39

The two samples' particles display similar shapes, as shown in Fig. 2. They accumulate with each other, and have a size of less than 1.0 μm.

Fig. 3 exhibits the samples' HRTEM images. The $Li[Li_{0.23}Ni_{0.15}Mn_{0.62}]O_2$ sample consists of bigger crystallites with a size of ~200 nm than the Al-doped one (~150 nm) (Figs. 3a and 3b). The magnified crystallites show the particles' well-ordered layered structures with a lattice distance of 0.47 and 0.43 nm, respectively (Figs. 3c and 3d). The diffraction patterns in Figs. 3e and 3f indicate a typical hexagonal structure. These results agree with the results of XRD shown in Fig. 1.

Fig. 4 shows the samples' charge/discharge curves at a low current density of 20 mA g^{-1}. Their initial charge curve can be roughly divided into a slope line and a plateau. The voltage plateau of Al-doped sample (~4.22 V) is higher than that of un-doped one (~3.80 V), implying their different

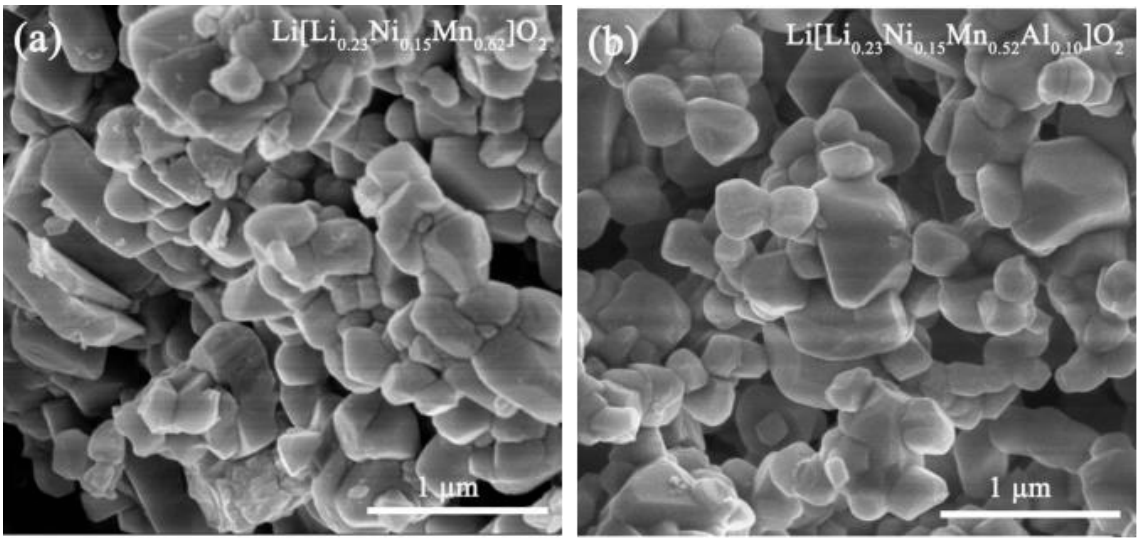

Figure 2. SEM images for (a) Li $[Li_{0.23}Ni_{0.15}Mn_{0.62}]O_2$, and (b) $Li[Li_{0.23}Ni_{0.15}Mn_{0.52}Al_{0.10}]O_2$.

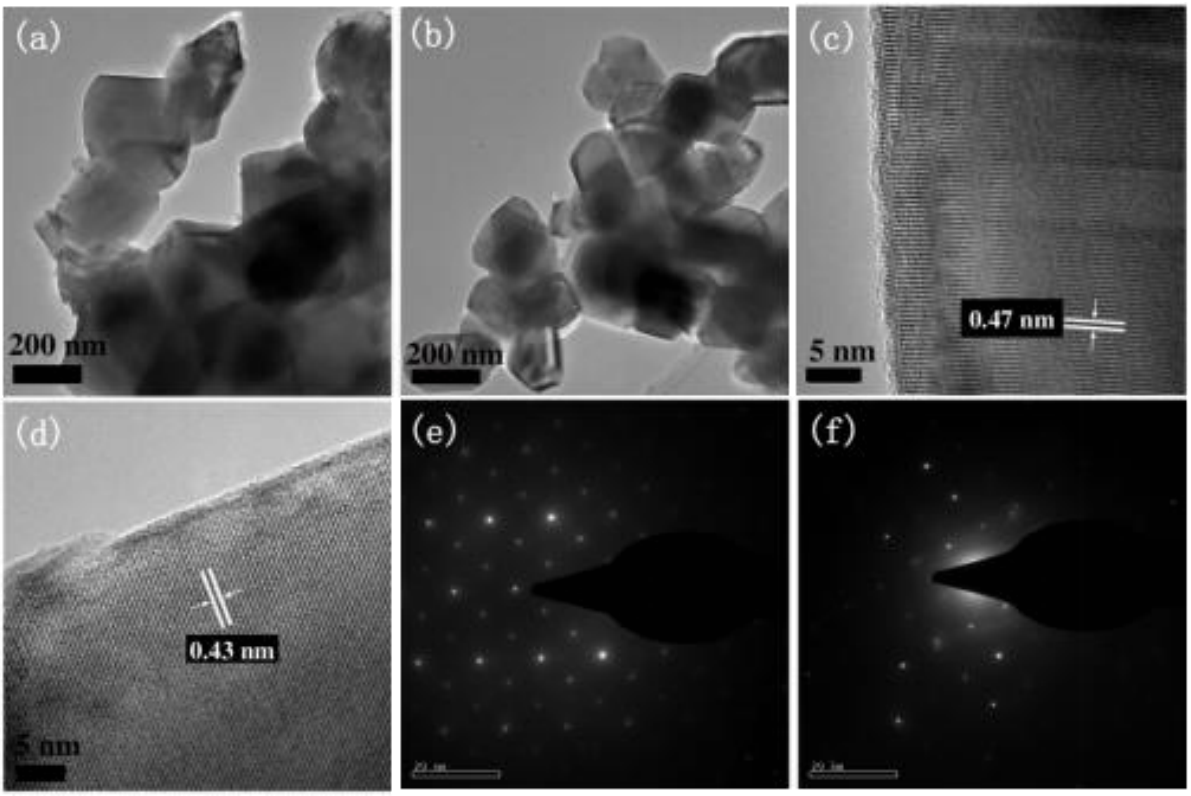

Figure 3. TEM images for (a) $Li[Li_{0.23}Ni_{0.15}Mn_{0.62}]O_2$, and (b) $Li[Li_{0.23}Ni_{0.15}Mn_{0.52}Al_{0.10}]O_2$; HRTEM images for (c) Li $[Li_{0.23}Ni_{0.15}Mn_{0.62}]O_2$, and (d) $Li[Li_{0.23}Ni_{0.15}Mn_{0.52}Al_{0.10}]O_2$; Diffraction patterns for (e) Li $[Li_{0.23}Ni_{0.15}Mn_{0.62}]O_2$, and (f) $Li[Li_{0.23}Ni_{0.15}Mn_{0.52}Al_{0.10}]O_2$.

properties. The discharge capacity of $Li[Li_{0.23}Ni_{0.15}Mn_{0.62}]O_2$ slowly increases from 65 to 200 mAh g^{-1} during 50 cycles. Whereas, the Al-doped sample keeps a relative stable capacity (>180 mAh g^{-1}) after the initial charge. Its charge/discharge curves almost overlap since the second cycle. The capacity loss of $Li[Li_{0.23}Ni_{0.15}Mn_{0.62}]O_2$ during the first cycle is 745 mAh g^{-1}, which is much larger than that of the Al-doped sample (65 mAh g^{-1}). The irreversible capacity loss mainly originates from the lithium loss due to the formation of solid electrolyte interface (SEI) layers [8,27]. Some oxygen resulted from the decomposition and rearrangement of lithium-rich oxide participates in the formation of SEI layers. The experimental results indicate that the Al-doped sample has a more stable structure, and exhibits more stable capacities during cycling.

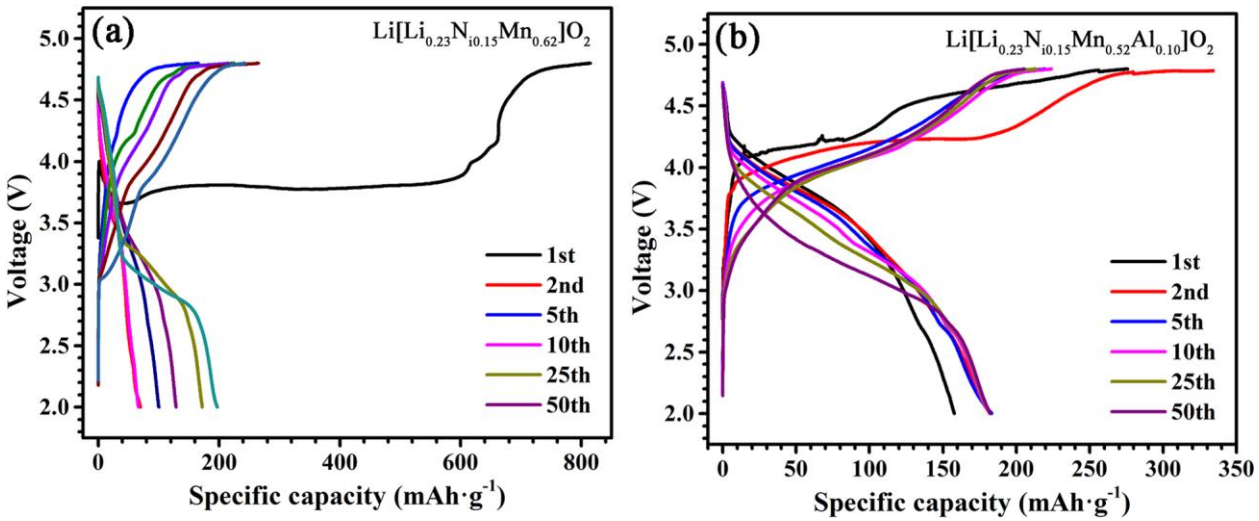

Figure 4. Charge/discharge curves of the samples in a voltage range of 2.0−4.8 V at 20 mA·g^{-1} for (a) $Li[Li_{0.23}Ni_{0.15}Mn_{0.62}]O_2$, and (b) $Li[Li_{0.23}Ni_{0.15}Mn_{0.52}Al_{0.10}]O_2$.

The cyclic voltammetry is used to study the oxidation/reduction of cathode material during cycling. As shown in Fig. 5, during the initial charge, either sample shows an oxidation peak at >4.70 V, which originates from the oxygen loss and crystal structure arrangement of the lithium-rich oxides. The $Li[Li_{0.23}Ni_{0.15}Mn_{0.62}]O_2$ sample exhibit two oxidation/reduction peak couples at ~3.0 V/2.7 V and ~4.5 V/4.0 V, which are attributed to the redox of Mn^{3+}/Mn^{4+} and Ni^{2+}/Ni^{4+}, respectively [27]. The Al-doped sample also display two similar oxidation/reduction peak couples. Therefore, we think that the doping aluminum is electrochemical inactive during cycling. In the first cycle, the oxidation peaks has a larger area than the reduction peaks, indicating the irreversible capacity loss. In subsequent cycles, the two areas of oxidation peaks and reduction peaks close to unity along with the improved reversible capacity.

Fig. 6 shows the samples' cycling performance. Compared with $Li[Li_{0.23}Ni_{0.15}Mn_{0.62}]O_2$, the Al-doped sample display more stable capacities during the cycling, indicating its well reversible lithium insertion/de-insertion. The $Li[Li_{0.23}Ni_{0.15}Mn_{0.62}]O_2$ sample's unstable capacity increases with the increasing cycle number, and reach the discharge capacity of 203 mAh g^{-1} during the 52th cycle.

The samples' rate performance is shown in Fig. 7. Both samples' discharge capacities rapidly decay with an increasing current density from 20 to 600 mA g^{-1}. For $Li[Li_{0.23}Ni_{0.15}Mn_{0.62}]O_2$, the

discharge capacity drops from 120 mAh g^{-1} to 13 mAh g^{-1}. The Al-doped sample exhibits better rate performance. Its discharge capacities decrease from 194 to 42 mAh g^{-1} with the increasing current. As the current density drops back to 20 mA g^{-1}, the Al-doped sample quickly regains a discharge capacity of 187 mA g^{-1} with capacity retention of 96.4%. Generally, the Al-doped sample has a higher discharge capacity than $Li[Li_{0.23}Ni_{0.15}Mn_{0.62}]O_2$ during cycling.

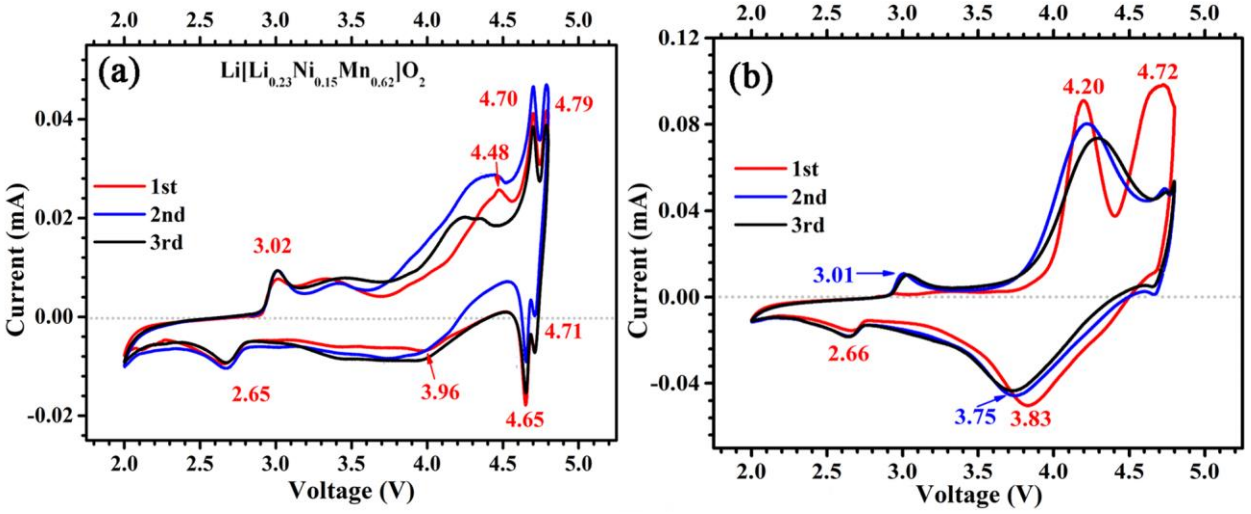

Figure 5. Cyclic voltammetry curves of the samples in a voltage range of 2.0–4.8 V for (a) $Li[Li_{0.23}Ni_{0.15}Mn_{0.62}]O_2$, and (b) $Li[Li_{0.23}Ni_{0.15}Mn_{0.52}Al_{0.10}]O_2$.

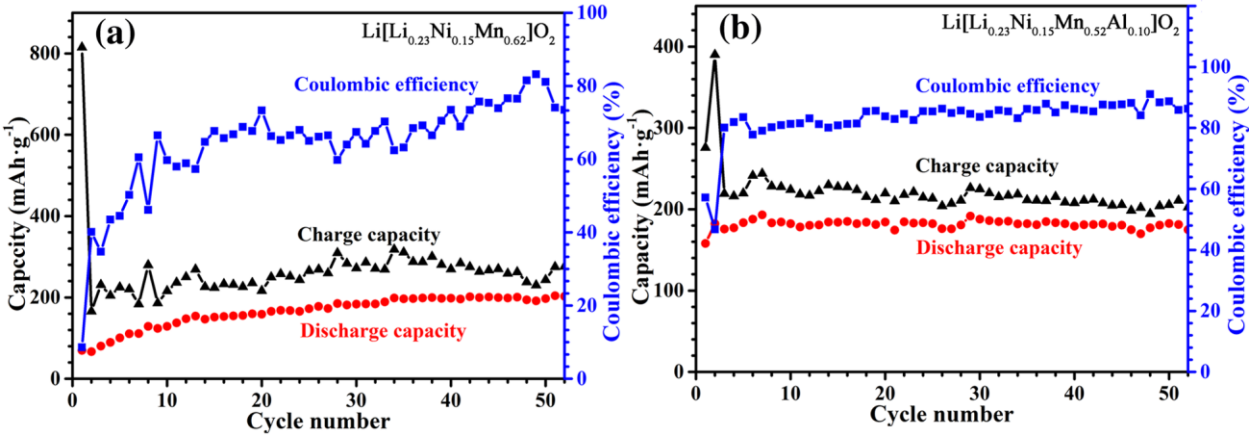

Figure 6. Cycling performance of the samples at 20 mA·g^{-1} for (a) $Li[Li_{0.23}Ni_{0.15}Mn_{0.62}]O_2$, and (b) $Li[Li_{0.23}Ni_{0.15}Mn_{0.52}Al_{0.10}]O_2$.

The Al-doped sample shows improved rate capacities and better stability during cycling. It is widely accepted that lithium-rich layered oxide is built by transition metal layers and lithium layers. The transition metal layer consists of MO_6 (M = Mn, Ni, Li) octahedra. All transition metal and the "rich lithium" are located in the transition metal layers [25−27]. Therefore, the doped aluminum substitutes partial manganese, and enters the transition metal layer. Aluminum ion keeps a fixed

valence state during charging/discharging, and reduces or buffers the Jahn-Teller distortion of Mn^{3+}. As a result, $Li[Li_{0.23}Ni_{0.15}Mn_{0.52}Al_{0.10}]O_2$ displays improved stability and better rate performance.

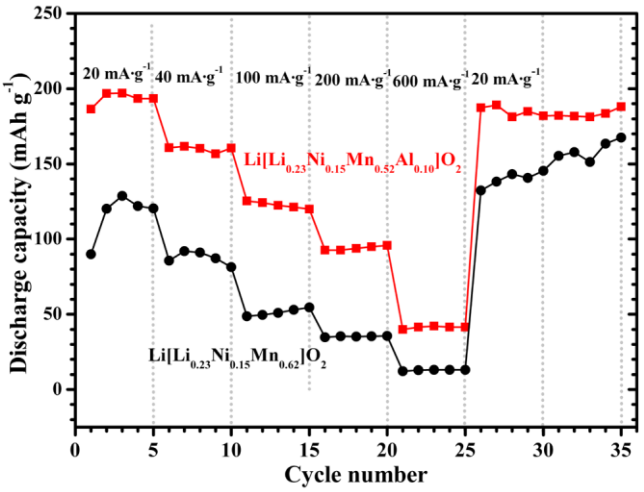

Figure 7. Rate performance of the samples at a current density between 20 and 600 mA g^{-1}: (a) $Li[Li_{0.23}Ni_{0.15}Mn_{0.62}]O_2$; (b) $Li[Li_{0.23}Ni_{0.15}Mn_{0.52}Al_{0.10}]O_2$.

There are some investigations about the doped lithium-rich layered oxides. Common doped elements include Co, Al, F, Mg, and Fe. Their effects are different. Kim *et al* [29] ascribed the improved capacity and rate capability of Co-doping $Li[Li_{0.1}Ni_{0.3}Co_{0.1}Mn_{0.5}]O_2$ to the reduced resistance of electrode. Park *et al* [8] found that Al doping prevents the structural degradation of $Li[Li_{0.15}Ni_{0.245}Al_{0.06}Mn_{0.545}]O_2$ during cycling, which delivered a discharge capacity of >200 mAh g^{-1} during cycling. F often is used to substitute O. A small amount (<5 mol%) of Al or/and F doping may result in the decreased irreversible oxygen loss during the first charge [30]. Therefore, Al or/and F doping may prove a useful way to control and tune the irreversible oxygen loss and capacity of lithium-rich layered oxides. However, less oxygen loss caused by Al or/and F doping means less lithium being extracted during the first charge. As a result, the Al/F mono-doping or co-doping often leads decreasing discharge capacities. Nevertheless, the doped lithium-rich layered oxides' structural and electrochemical stability often be improved. Huang *et al* [31] found that the Mg-doped $Li_{1.2}[Mn_{0.54}Ni_{0.13}Co_{0.13}]_{0.99}Mg_{0.01}O_2$ exhibits a higher capacity retention (~83%) compared with the un-doped $Li_{1.2}[Mn_{0.54}Ni_{0.13}Co_{0.13}]O_2$ with a value of 54% in the 100th discharge at a current density of 250 mA g^{-1}. They considered that Mg doping could reduce the barrier during the Li^+ transferring and stabilizes the crystal structure. Li *et al* [32] reported that the Fe-doped $Li[Li_{0.23}Mn_{0.47}Fe_{0.2}Ni_{0.1}]O_2$ cathode material presents high capacities and a nice capacity retention of 97% after 20 cycles at different rate. Both XPS and first principles studies done by Laisa *et al* [33] reveal that the doped Fe in $Li_{1.2}Ni_{0.13}Fe_{0.13}Mn_{0.54}O_2$ participated in the Fe^{+3}/Fe^{+4} redox during charging/discharging. The Fe-doped cathode material exhibits a discharge capacity of ~200 mAh g^{-1}.

The results in this study reveal that the doped aluminum did participate in the formation of lithium-rich layered oxide. Although the doped aluminum did not show obvious redox during cycling, it enhances the structural and electrochemical stability of the lithium-rich layered oxide.

4. CONCLUSIONS

In this study, the Al-doped lithium-rich oxide $Li[Li_{0.23}Ni_{0.15}Mn_{0.52}Al_{0.10}]O_2$ is synthesized successfully, and consists of well-order crystallites with a layered structure. As cathode material for lithium-ion batteries, the Al-doped sample exhibits better cycling and rate performance than $Li[Li_{0.23}Ni_{0.15}Mn_{0.62}]O_2$ during cycling. The doped aluminum does not change its valence state during cycling. However, it enhances the structural stability and rate performance of the lithium-rich layered oxide cathode material.

ACKNOWLEDGEMENTS
This research is supported by the National High Technology Research and Development Program of China (863) (2013AA050905, 2014AA052301), the National Nature Science Foundation of China (51172160, 50902102) and NSF of Tianjin City (11JCYBJC07500).

References

1. T. Sasaki, Y. Ukyo, P. Novák, *Nat. Mater*. 12 (2013) 569.
2. M.E. Spahr, P. Novák, O. Haas, R. Nesper, *J. Power Sources* 68 (1997) 629.
3. J. Fan, P.S. Fedkiw, *J. Power Sources* 72 (1998) 165.
4. A.R. Armstrong, P.G. Bruce, *Nature* 381 (1996) 499.
5. Q. Liu, Y. Li, Z. Hu, D. Mao, C. Chang, F. Huang, *Electrochim. Acta* 24 (2008) 7298.
6. I. Taniguchi, D. Song, M. Wakihara, *J. Power Sources* 109 (2002) 333.
7. S.H. Kang, J. Kim, M.E. Stoll, D. Abraham, Y.K. Sun, K. Amine, *J. Power Sources* 112 (2002) 41.
8. S.H. Park, Y.K. Sun, *J. Power Sources* 119–121 (2003) 161.
9. C.J. Han, J.H. Yoon, W.I. Cho, H. Jang, *J. Power Sources* 136 (2004) 132.
10. S.T. Myung, S. Komaba, N. Hirosaki, K. Hosoya, N. Kumagai, *J. Power Sources* 146 (2005) 645.
11. D. Li, Y. Sasaki, M. Kageyama, K. Kobayakawa, Y. Sato, *J. Power Sources* 148 (2005) 85.
12. S.K. Martha, H. Sclar, Z.S. Framowitz, D. Kovacheva, N. Saliyski, Y. Gofer, P. Sharon, E. Golik, B. Markovsky, D. Aurbach, *J. Power Sources* 189 (2009) 248.
13. X. Ding, H. Zhou, G. Liu, Z. Yin, Y. Jiang, X. Wang, *J. Alloys Compd.* 632 (2015) 147.
14. H. Kobayashi, Y. Arachi, S. Emura, K. Tatsumi, *Solid State Ionics* 178 (2007) 1101.
15. S. Dou, W.L. Wang, H. Li, X. Xin, *J. Solid State Electrochem.* 15 (2011) 747.
16. S.P. Woo, S.H. Lee, K.S. Lee, Y.S. Yoon, *Mater. Lett.* 129 (2014) 80.
17. S.H. Kang, K. Amine, *J. Power Sources* 119–121 (2003) 150.
18. D. Li, Y. Sasaki, K. Kobayakawa, Y. Sato, *J. Power Sources* 157 (2006) 488.
19. A.E. Abdel-Ghany, A. Mauger, H. Groult, C.M. Julien, *Ionics* 18 (2012) 241.
20. A.R. Armstrong, M. Holzapfel, P. Novák, C.S. Johnson, S.H. Kang, M.M. Thackeray, P.G. Bruce, *J. Am. Chem. Soc.* 128 (2006) 8694.
21. K.A. Jarvis, Z. Deng, L.F. Allard, A. Manthiram, P.J. Ferreira, *Chem. Mater.* 23 (2011) 3614.
22. J.X. Wang, L. Wang, X.M. He, J.J. Li, Z.J. Dai, J.L. Wang, *Int. J. Electrochem. Sci.* 11 (2016) 333.
23. N. Ishida, H. Hayakawa, H. Shibuya, J. Imaizumi, J. Akimoto, *J. Power Sources* 244 (2013) 505.
24. Y.J. Zhang, Z.Z. Shi, H.R. Mao, Z.P. Qiu, C.Y. Yang, H.B. Luo, P. Dong, *Int. J. Electrochem. Sci.* 12 (2017) 3782.
25. M. Jiang, B. Key, Y.S. Meng, C.P. Grey, *Chem. Mater.* 21 (2009) 2733.
26. C.C. Wang, K.A. Jarvis, P.J. Ferreira, A. Manthiram, *Chem. Mater.* 25 (2013) 3267.
27. R.M. Gu, S.Y. Yan, S. Sun, C.Y. Wang, M.W. Li, *J. Solid State Electrochem.* 19 (2015) 1659.

28. A. Tang, K. Huang, *Mater. Chem. Phys.* 93 (2005) 6.
29. J.-H. Kim, C.W. Park, Y.-K. Sun, *Solid State Ionics* 164 (2003) 43.
30. Y. Wu, A. Manthiram, *Electrochem. Solid-State Lett.* 10 (2007) A151.
31. Z. Huang, Xinhai Li, Y. Liang, Z. He, H. Chen, Z. Wang, H. Guo, *Solid State Ionics* 282 (2015) 88.
32. J. Li, L. Wang, L. Wang, J. Luo, J. Gao, J. Li, J. Wang, X. He, G. Tian, S. Fan, *J. Power Sources* 244 (2013) 652.
33. C.P. Laisa, A.K. Nanda Kumar, S. Selva Chandrasekaran, P. Murugan, N. Lakshminarasimhan, R. Govindaraj, K. Ramesha, *J. Power Sources* 324 (2016) 462.